Tightly-coupled GIS data in GNSS fix computations with integrity testing

C. Fouque* and Ph. Bonnifait

Heudiasyc UMR CNRS 6599,
Université de Technologie de Compiègne,
Centre de recherche de Royallieu,
BP20529, 60205 Compiègne, Cedex, France
E-mail: clement.fouque@hds.utc.fr
E-mail: philippe.bonnifait@hds.utc.fr
*Corresponding author

Abstract: Global Navigation Satellite Systems (GNSS) are often used to localise a receiver with respect to a given map. This association problem, also known as map-matching, is usually addressed using estimated positions computed by the GNSS receiver. In this paper we propose a method that combines the cartographic data in the GNSS computation fix itself. We focus on the use of a road network provided by cartographers such as NavTeQ or TeleAtlas. Geo-referenced data is modelled by segments that can be used as constraints or fused with the pseudo-ranges. Using residuals, a new method for tackling the underlying problem of the road selection is proposed. We show that this approach is also well adapted to the integrity problem of map-matching, since a consistency test is derived. Experimental results illustrate the performance of this method with different maps.

Keywords: outdoor localisation; global navigation satellites systems; GNSS; GIS data; tightly coupled data fusion; integrity monitoring.

Reference to this paper should be made as follows: Fouque, C. and Bonnifait, Ph. (2008) 'Tightly coupled GIS data in GNSS fix computations with integrity testing', *Int. J. Intelligent Information and Database System*, Vol. 2, No. 2, pp.167–186.

Biographical notes: Clément Fouque (1982) obtained his Masters Degree in Robotics from the Université Pierre et Marie Curie (Paris VI), France, in 2006. Since December 2006, he has been at Heudiasyc UMR 6599, France, as a PhD student in Computer Science and Engineering at the Université de Technologie de Compiègne (UTC). His current research interests are multi-sensor fusion (geo-referenced data, GNSS and INS), integrity-monitoring and map-matching for localisation for intelligent vehicles and advanced driving assistance systems.

Philippe Bonnifait (1969) graduated from the Ecole Superieure d'Electronique de l'Ouest, France, in 1992 and obtained his PhD Degree in automatic control and computer science from the Ecole Centrale de Nantes, France, in 1997. In December 2005, he obtained his Habilitation à Diriger des Recherches from the Université de Technologie de Compiègne (UTC). Since September 1998, he has been at Heudiasyc UMR 6599, France,

and he is currently Professor in the UTC's Computer Science and Engineering Department. His current research interests are in intelligent vehicles and advanced driving assistance systems, with particular emphasis on dynamic ego-localisation based on multisensor-fusion (GNSS, dead-reckoning and GIS).

1 Introduction

Global Navigation Satellite Systems (GNSS) including GPS, Glonass and Galileo, along with their Satellite-Based Augmentation Systems (SBAS) such as WAAS, EGNOS and MSAS, are very promising affordable technologies for many applications. Very often, absolute positioning is useful when it is associated with a geographical database that contains a priori information. A good example is a GPS-based navigation system that uses the road network information for route planning or for contextual information retrieval, such as road curvature estimation, speed limits if they are stored, or Points of Interest (POI). However, Geographical Information (GI) can be extremely rich. For instance, GI can describe terrain elevation, location of buildings, ground vegetation, rivers, etc. GI is spatially-indexed and handled by Geographic Information Systems (GIS) that allow the different GI layers to be accessed, elements to be added or modified, coordinate transforms to be computed, projections to be applied and information to be displayed. The quantity of available GI is increasing rapidly, and it can be used in the localisation process itself as a priori knowledge of the environment. Moreover, in some applications, this information can contain natural landmarks stored as GI and used for precise positioning in urban areas (Jabbour et al., 2006; Meizel et al., 2005).

The problem of localising a receiver with respect to a map is known as map-matching. Usually this problem is tackled using GNSS fixes provided by a receiver, i.e., position solutions computed using pseudo-ranges and ephemerid data. The GNSS data is often fused with dead-reckoning in order to improve positioning availability and accuracy (Lahrech et al., 2005; Meizel et al., 2005). The main drawback of this approach is the necessity for DR sensors and at least four satellites in line of sight, conditions which are rarely satisfied in urban canyons (Georgiev and Allen, 2004). Moreover, integrity monitoring is difficult to assess in such cases, as the pseudo-range measurements can suffer from multipath. An alternative is a tightly-coupled approach in which the map information is used in the computation of the fix. This approach, which also allows the mixing of GPS, Glonass or Galileo pseudo-ranges and multipath mitigation (Betaille et al., 2003), is the one addressed in this paper.

We focus on the use of a map of the road network provided by cartographers such as NavTeQ or TeleAtlas. The available information describes the centre-lines of carriageways in a 2D representation. The main difficulty is using such information in the GNSS computation. To this end we propose the construction of a navigation frame in which the position of the satellites at their transmission time is known. By first supposing that the road is known, we show how to compute a location (Fouque and Bonnifait, 2007). We then present a strategy for selecting the most likely road by using the residuals of the computation. These residuals also allow an integrity test to be performed. Monitoring the positioning integrity is indeed crucial for many land vehicle

applications (Santa et al., 2006). Experimental results carried out with our experimental car show the performance of the approach: If more than three satellites are visible, we can apply an integrity test that quantifies the confidence in the map-matched location.

The paper is organised as follows. Section 1 provides a reminder of how a GPS fix is computed. Several methods for map-aided GPS positioning (provided that the road on which the vehicle is travelling is known) are then described in Section 2. In Section 3 a candidate segments algorithm is presented, and in Section 4 we propose an integrity analysis for selecting the most likely road. Section 5, our conclusion, presents real experimental results obtained using the proposed road selection algorithm to realise an integrity test of the map-aided GNSS positioning.

2 Absolute GNSS positioning

We start by introducing geographical information into the position computation. GI is frequently used in a dynamic state observation process such as Kalman filtering, either as an observation (Jabbour et al., 2006), or indirectly, using a camera to detect precisely-charted marked lanes (Laneurit et al., 2005). In this work we adopt a static approach without state filtering: all the measurements are processed simultaneously when they are available. To illustrate the use of GI in GNSS computation let us consider a standard digital road map. In this section we present two ways of including cartographic data, assuming that the vehicle is on a road and that the segment in which it is currently located is known.

2.1 Estimated positions of SVs

SVs broadcast ephemerid data in real-time, and these include Keplerian parameters describing their orbits. Given a GPS timestamp t_e^i, it is possible to compute an estimated position of SV^i at this time index in the ECEF(t_e^i), since ECEF rotates with earth. The receiver has to solve the following problems:

- What is the transmission time t_e^i of the sequence sent by SV^i ?
- What was the position SV^i at time t_e^i in ECEF(t_e^i)?
- What is the position in the current ECEF?

The receiver estimates the time of flight t_{flight}^i of the sequence broadcast by SV^i, by measuring the shift between the transmitted frame and its locally-generated replica (C/A code):

$$t_{flight}^i = t_r - t_e^i \tag{1}$$

where t_r is the reception time and t_e^i is the transmission time in the GPS time reference system. t_{flight}^i is in the order of 70 ms. Unfortunately, there is an internal clock bias in the receiver with respect to the GPS reference time. At the reception time the receiver reads its clock $t_u(t_r)$. We have:

$$t_r = t_u(t_r) + dt_u. \tag{2}$$

The transmission time is therefore given by:

$$t_e^i = t_u(t_r) + dt_u - t_{flight}^i. \tag{3}$$

If the internal clock bias of the receiver is kept small, then t_e^i can be approximated by

$$t_e^i \approx t_u(t_r) - t_{flight,measured}^i \tag{4}$$

where $t_{flight,measured}^i$ is the measurement of the time of flight for SV^i. Using t_e^i, it is possible to compute an estimated position ${}^{ECEF(t_e^i)}X_{sat}^i = (x^i(t_e^i), y^i(t_e^i), z^i(t_e^i))$ of SV^i in the frame ECEF(t_e^i) using the broadcast ephemerid. See Kaplan (1996) for details. We now need to express the SV position at transmission time t_e^i in ECEF(t_r). It will be denoted ${}^{ECEF(t_r)}X_{sat}^i(t_e^i)$. If we model the earth's rotation by a simple 24-hour periodic rotation around z axis (ECEF coordinates), then we have

$$\alpha_{earth}^i = \omega_{earth} \cdot t_{flight,measured}^i \tag{5}$$

$${}^{ECEF(t_r)}X_{sat}^i = Rot(z, -\alpha_{earth}^i) \cdot {}^{ECEF(t_e^i)}X_{sat}^i. \tag{6}$$

For reasons of simplicity we shall hereafter omit the superscript ECEF(t_r), since the entire computation is done in this frame.

2.2 Receiver position computation

To compute the position of the receiver, let us now consider the pseudo-range measurement ρ^i made by the receiver on SV^i:

$$\rho^i = c \cdot t_{flight,measured}^i. \tag{7}$$

Like the receiver, SV^i has a clock offset:

$$t_e^i = t_s(t_r) + dt_s^i. \tag{8}$$

We can therefore rewrite the pseudo-range measurement as:

$$\rho^i = c \cdot (t_r - t_e^i) + c \cdot (dt_u - dt_s^i) \tag{9}$$

where c is the speed of light in a vacuum. Let R^i denote the geometrical distance between SV^i and the receiver in ECEF(t_r) frame:

$$R^i = \sqrt{(x - x^i(t_e^i))^2 + (y - y^i(t_e^i))^2 + (z - z^i(t_e^i))^2} \tag{10}$$

$$R^i = c \cdot (t_r - t_e^i). \tag{11}$$

To simplify matters, let us assume that dt_s^i can be precisely known using the ephemerid data and SBAS (EGNOS, WAAS, or MSAS) corrections. The corrected pseudo-range ρ_c^i is obtained using equation (9):

$$\rho_c^i = R^i + c \cdot dt_u. \tag{12}$$

Using equations (10) and (12), a relationship is constructed between the corrected pseudo-range measurement for an SV on the one hand, and both the receiver position and its internal clock bias on the other. Assuming n visible SVs, a non-linear equation system can be written:

$$\rho_c^i = h^i(x, y, z, dt_u), \quad \forall i = 1, \ldots, n. \tag{13}$$

If $n > 4$, then the system is also redundant, involving static positioning that can be solved using an iterative Least-Squares method (hereafter termed Newton-Raphson) (Kaplan, 1996), or alternatively Bancroft's non-iterative method, which we shall not describe here, but instead we refer the reader to Yang and Chen (2001).

2.3 Weighted Least-Squares solution

Let us define the state vector s as:

$$s = [x, y, z, dt_u]^t. \tag{14}$$

Using SBAS-broadcast estimated-noise covariance data, it is possible to build the noise covariance matrix used in a weighted Least-Squares solution. Assuming that the measurement errors are not correlated, this matrix (denoted W) has the form:

$$W = \begin{bmatrix} \sigma_1^2 & & 0 \\ & \ddots & \\ 0 & & \sigma_n^2 \end{bmatrix}. \tag{15}$$

If the receiver is unable to provide such data, the weight matrix W can be estimated using the Signal-Noise Ratio (SNR) and the elevation angle ϕ of each satellite in line of sight.

The Newton-Raphson iterative solver consists in linearising the system around the current estimated state $\hat{s}_0$:

$$ds = H^+(\hat{s_0}) \cdot (\rho_c - h(\hat{s_0})) \tag{16}$$

$$\hat{s} = \hat{s}_0 + ds \tag{17}$$

where $H^+(\hat{s_0})$ is the weighted generalised inverse of the Jacobian matrix corresponding to the observation equation defined by equation (13). $H^+(\hat{s_0})$ is given by:

$$H^+(\hat{s_0}) = [H^t(\hat{s_0}) \cdot W^{-1} \cdot H(\hat{s_0})]^{-1} \cdot H^t(\hat{s_0}) \cdot W^{-1}$$

$$H(\hat{s_0}) = \left.\frac{\partial h}{\partial s}\right|_{\hat{s_0}}. \tag{18}$$

The final estimated solution is obtained when the method has converged towards a fixed point.

3 GIS data in the GNSS computation

We shall now introduce geographical information into the position computation. To illustrate this concept, let us use a digital road map. Supposing that the vehicle is on a road and that the segment in which it is currently located is known, we here present two ways of including cartographic data.

3.1 Road maps

A road map is a database that contains a vectorial description of the road network. Roads are described in a discrete fashion by their centre-lines. Data associated with a road are classified into three groups:

- *Geographical information*: A segment set describing the geometry of the road.
- *Topological information*: Description of connectivity between road segments.
- *Semantic information*: Road name, speed limit, etc...

Digital road maps can achieve a metrical precision, which is sufficient for many navigation tasks including route planning. To help overcome memory and real-time constraints, the system usually has in memory a cache of the roads around the current position of the vehicle (typically 1 Km^2).

3.2 Working frame

In order to compute a valid tightly-coupled GNSS/map-matching positioning solution, a common working frame is necessary. Let us recall that GPS provides ephemerid data in the WGS84 Cartesian frame, whereas maps depict roads as part of the earth's surface. Consequently, map nodes and shape points are only described by their longitude and latitude, assuming their elevation equals 0.

Using the geographical data from the map, let us determine a tridimensional local frame (denoted loc) such that its plane (O, i, j) is tangential to the WGS84 earth reference ellipsoid. First, the map's point coordinates are converted from the geodetic WGS84 to the Cartesian WGS84 frame. The origin O is chosen to correspond to the origin node of a road close to the estimated position. The i axis was made to correspond to the first segment of this road and the (O, i, j) plane is characterised by a geometry point of any other nearby road, provided that this point is not situated on the i axis. Finally, the k axis is chosen such that the local frame is right-handed.

A homogeneous transform ${}^{loc}T_{WGS84}$ is then computed. It contains the rotation and translation terms needed to apply the transform. Using ${}^{loc}T_{WGS84}$, the satellite coordinates and the map cache, geometry points can be converted in the working frame:

$$ {}^{loc}\begin{bmatrix} x \\ y \\ z \\ 1 \end{bmatrix} = {}^{loc}T_{WGS84} \cdot {}^{WGS84}\begin{bmatrix} x \\ y \\ z \\ 1 \end{bmatrix} . \tag{19} $$

It should be noted that the working frame is temporary (typically for a road cache) and valid only for small regions (limited to several kilometers), which addresses the meridian convergence problem.

3.3 Plane constraint for computation

Let suppose that the correct road segment has been selected from the road points given by the GIS. The constraint defined by this selected segment is part of a vertical plane (in the working frame), since the elevation of the map is unknown. In practice, we consider the whole plane and we check afterwards that the result matches the segment.

Taking $A(a_1, a_2)$ and $B(b_1, b_2)$ as the extremities of the segment, the segment defines a straight line whose equation is

$$\begin{cases} y = b_1 + \frac{b_2 - a_2}{b_1 - a_1} \cdot (x - a_1) & \text{if } b_1 \neq a_1 \\ x = a_1 & \text{otherwise} \end{cases}. \tag{20}$$

For simplicity we shall consider only the general case $b_1 \neq a_1$. The geometrical equation (20) means that only the computation along (x, y) is constrained. This can be expressed as

$$y = f_1(x) \quad \text{if } b_1 \neq a_1. \tag{21}$$

3.4 First method: unknown elimination

This method was proposed by Cui and Ge (2003). The idea is to eliminate a variable using the constraint equation. Introducing equation (21) in equation (10), the geometrical distance between the receiver and SV ^{i} can be rewritten as

$$R^i = \sqrt{(x - x^i(t_e^i))^2 + (f_1(x) - y^i(t_e^i))^2 + (z - z^i(t_e^i))^2}. \tag{22}$$

This new expression of the geometrical distance gives a new non-linear system:

$$\rho_c^i = g^i(x, z, dt_u), \quad \forall i = 1, \ldots, n. \tag{23}$$

The dimension of the problem has now been reduced, and the minimum number of SVs necessary for computing the positioning solution is 3. Since the constraint is strong, the computed position belongs to the constraint plane. It should be noted that its projection onto the map plane can be outside the segment.

3.5 Second method: plane fusion

This method was proposed by Syed and Cannon (2005). Using the segment parameters, a new observable is built. It therefore becomes possible to add a new equation to the observation model defined using equation (10). Let us define the pseudo-measurement ρ_c^{n+1} extracted from the GIS data and its associated observation equation:

$$\begin{aligned} &(b_1 - a_1) \cdot a_2 + (a_2 - b_2) \cdot a_1 = (b_1 - a_1) \cdot y + (a_2 - b_2) \cdot x \\ &\rho_c^{n+1} = h^{n+1}(x, y, z, dt_u). \end{aligned} \tag{24}$$

Thus, an extended observation model can be written as:

$$\tilde{\rho}_c = \tilde{h}(s). \tag{25}$$

with s the state vector given in Section 2.3 and $\tilde{\rho}_c = [\rho_c, \rho_c^{n+1}]^t$.

Using this additional measurement and at least three SVs, the positioning solution can be computed. In contrast to the unknown elimination method, the computed solution is not situated within the constraint plane defined by the road segment.

Moreover, it is possible to extend the weighted Least-Squares solution described in Section 1.3 in order to compute the matched fix. A weight can therefore be ascribed to the GIS data as an indicator of its quality. From Section 1.3, the matched approximate solution $\hat{s}_m$ can be expressed by

$$\hat{s}_m = \widetilde{H}^{+}(\hat{s}_m) \cdot (\rho_c - \tilde{h}(\hat{s}_m)) \tag{26}$$

with

$$\widetilde{H}(\hat{s}_m) = \left.\frac{\partial \tilde{h}}{\partial s}\right|_{\hat{s}_m} \quad \widetilde{W} = \begin{bmatrix} W & 0 \\ 0 & \sigma_{GIS}^2 \end{bmatrix}. \tag{27}$$

where σ_{GIS} represents the map error.

We have seen how road segment information can be introduced into the positioning solution computation. A road selection algorithm is now proposed in order to select all the segments that match the current GNSS observations. The road selection comprises three steps. First, candidate segments are extracted from the road cache. Then candidate segments that fail to match a consistency criterion are eliminated, and finally the most likely segment is selected.

4 Extraction of candidate segments

This first step of the road selection method involves the extraction of candidate segments from the road cache. For each segment, a tightly-coupled positioning solution is computed using the unknown elimination method, described above in Section 2.4, in order to determine the corresponding matched point. A non-linear equation system like equation (23) is therefore solved for each segment of the road cache using the Newton-Raphson iterative solver.

As we saw in Section 2.4, the provided solution is constrained to a vertical plane (along the k axis) defined by the road segment (which forms part of plane (O, i, j)). It follows that any segment is a candidate if it satisfies the two following conditions:

- The projection of the fix onto the reference plane (O, i, j) belongs to the segment. As the segment shape points are known, a simple test can be performed involving the projection of the fix onto the reference plane (O, i, j). Let us define the segment extremities M and N. Using a scalar product, the projection of the computed fix onto (O, i, j) (denoted P) belongs to the road segment if:

$$\vec{MP} \cdot \vec{NP} \leq 1 \tag{28}$$

- The altitude of the matched fix should be close to 0 in the working frame. We therefore apply a threshold (denoted Th_{alt}) in order to eliminate outlying solutions:

$$z < Th_{alt} \tag{29}$$

where z defines the altitude of the matched point in the working frame.

Using the conditions defined by equations (28) and (29), a set of candidate segments is obtained. Note that this step may yield no segments at all (when using wrong road cache, for instance), or a set of segments that do not correspond to the true road segment. This can occur if a large road cache is used.

5 Integrity of map-matching

Integrity methods suppose that there is a redundancy in the measurements (Belabbas and Gass, 2005). Using GIS data in the GNSS computation reduces the number of satellites required in line of sight. Either there are three unknowns and n measurements (see equation (23)), or there are four unknowns and $n + 1$ measurements (see equation (25)). So, with n satellites, the degree of redundancy is $n - 3$. We may therefore assume that at least four satellites are visible for monitoring integrity.

In this section the plane fusion method is used for integrity analysis, since it allows the veracity of a map to be weighted, unlike the unknown elimination method which cannot handle map errors. The integrity test that we consider here relies on a consistency check of residuals. Assuming that inconsistencies can result only from wrong matches (and not GNSS faults), this test allows the selection of the most likely segment, if it exists.

5.1 Positioning residuals

In order to determine whether or not a segment is consistent, the positioning residuals of the iterative Least-Squares solver are used. As this solver is iterative, the residuals vector is computed after convergence of the solution. Let rewrite equation (25) with the residuals vector ε:

$$\varepsilon = \tilde{\rho}_c - \tilde{h}(\hat{s}) \tag{30}$$

$\hat{s}$ is the last solver solution to have been estimated. Given the linearisation point $\hat{s}_0$ and the variation vector ds, the positioning residuals vector ε is:

$$\varepsilon = \tilde{\rho}_c - \tilde{h}(\hat{s}_0 + ds). \tag{31}$$

The expression of ds is given by equation (17) (this is the result obtained by the solver at the last step), where the pseudo-range measurement vector ρ_c is replaced by its extended version $\tilde{\rho}_c$, and the observation model h by $\tilde{h}$. Consequently, using a first-order linearisation, the residuals vector is now:

$$\varepsilon = \tilde{\rho}_c - \tilde{h}(\hat{s}_0) - \widetilde{H}(\hat{s}_0) \cdot ds. \tag{32}$$

It should be remarked that this is a weighted residuals vector.

5.2 Elimination of inconsistent segments

For each candidate segment, the Euclidean norm $\|\varepsilon\|$ of the weighted positioning residuals is computed from equation (32) using the results of the last iteration of the Newton-Raphson solver. In order to eliminate the inconsistent segments, a χ^2-test is performed for all the candidate segments under Gaussian assumptions (Walter and Enge, 1995). If the square norm of the residuals exceeds a certain threshold Th_{con} then the current candidate segment is eliminated. This strategy can be interpreted as a degenerated Receiver Autonomous Integrity Monitoring (RAIM) fault isolation, since we are assuming that it is always the candidate segment that is faulty, and never the GNSS measurements.

The problem is now to define the threshold Th_{con}. In our case, we consider that the pseudo-range noise can be different for each satellite in view of the SBAS correction, and also that the map error is known. In Belabbas and Gass (2005), the authors propose a Cholesky decomposition of $\widetilde{W}$ (see equation (27)):

$$\widetilde{W} = A \cdot A^t. \tag{33}$$

Let consider the new normalised positioning residuals ε':

$$\varepsilon' = A^{-1} \cdot \varepsilon. \tag{34}$$

A segment is therefore consistent if

$$\|\varepsilon'\| < Th_{con} \tag{35}$$

where Th_{con} is a threshold computed using the inverse of a χ^2 cumulative distribution function with $(n-3)$ degrees of freedom and a given P_{fa} (probability of false alarm). P_{fa} depends on the application. Let recall that n is the number of pseudo-range measurements used in the positioning computation.

This stage might yield no segments at all (if the vehicle is off-road, for instance), or several segments in the case of an ambiguous situation.

5.3 Segment selection

If there are no consistent segments, the fusion of the map with the GNSS data is not possible because the vehicle is probably not located on a road to be found within the cache. This fact is useful for detecting cache management problems. Otherwise, if there are several consistent segments, it becomes a question either of selecting the most likely segment, or of carrying out multi-hypothesis matching as in Cui and Ge (2003), involving Interacting Multiple Models (IMM) at each junction.

In order to select the most likely segment from a set of consistent segments, a simple strategy is to choose the one with the lowest positioning residuals norm. Let us study this strategy using real data.

6 Experimental results

6.1 Methodology

Experiments were carried out in two stages in July 2006. The first stage was the recording of data, and the second stage the processing of this data. Data was recorded using our Laboratory's experimental vehicle *Strada* (Figure 1) and a *Trimble 5700* GPS receiver in stand-alone mode. Data was recorded on roads near the lab which are well identified in the geographical database. SV measurements were recorded using *Rinex 2.10* observation file format and the corresponding navigation file was used. Using the Rinex files recorded by the receiver, a reference trajectory was computed in DGPS PPK mode using *Trimble Total Control* software and data from several reference stations (French Orpheon service).

Figure 1 HeuDiaSyC experimental vehicles: Carmen (*left*) and Strada (*right*)

For all experiments, a fixed road cache was extracted from a GIS database provided by two cartographers (*NavTeQ* and *TeleAtlas*). Hereafter we shall simply refer to these road caches as map$_i$, for reasons of non-disclosure. The road caches were extracted around the lab, with a diameter of about 600 m. The origin of the working frame was set to the same crossroads in each map.

In these experiments the weight matrix W and the extended weight matrix $\widetilde{W}$ were set to identity. This means that the standard deviation σ_i of the pseudo-ranges and the standard deviation σ_{GIS} of the map were assumed to be equal.

$$\sigma_i = \sigma_{GIS} = \sigma_{UERE}. \tag{36}$$

The integrity threshold Th_{con} was computed using a P_{fa} such that one false alarm per hour is permitted, which would seem acceptable for many land vehicle applications ($P_{fa} = 2.75 \times 10^{-4}$). Given this simplification, the integrity test equation (35) is reduced to:

$$\|\varepsilon'\| < \sigma_{UERE} \cdot \sqrt{Th_{con}}. \tag{37}$$

The constellation state at the beginning of the data recording was plotted using a skyplot graphic (Figure 2), which allows their elevation and azimuth angles respectively to be estimated with respect to the local.

Figure 2 GPS constellation recorded at the start of the road test

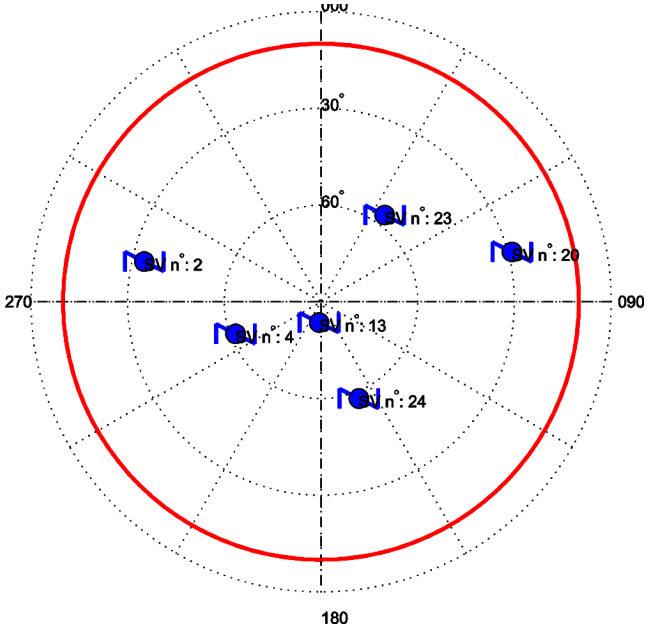

6.2 *Static tests*

In this section we analyse the road selection algorithm and the tightly-coupled GNSS-Map fusion using a single fix. The candidate segment extraction and the integrity test are computed for the same position, and the results are compared to the reference PPK DGPS fix. For this test map biases were removed and all the visible satellites were used. For simplicity, the local frame was made to correspond to the nearest road junction. The (O, i) axle coincides with one of the segments composing this road junction. In reality this segment is not East-oriented.

The results of the candidate segment selection process are shown in Figures 3 and 4 shows the results of the road selection. 10 road candidate segments satisfy the requirements. One remarks that several candidates are near to reference PPK DGPS fix (about 50 m), but that some others, lying further away, have been also chosen. This may at first seem surprising, but when one recalls that the diameter of the road cache is small with respect to the satellite distances, the result appears coherent, since the segments are only 300 m away from the reference fix.

The integrity test in Section 5, when applied to the candidate segments, yields only two (cf. Figure 4). Let consider a stand-alone GPS fix computed using the Least-Squares method. We can see that the vehicle is located near a road junction, which gives rise to an ambiguous situation, where the two consistent segments are those composing the road junction. Moreover, the most likely segment is effectively the vehicle's current segment.

6.3 *Dynamic tests*

In this section we present computation results for matched positions obtained during a dynamic test using all the visible satellites (5 in this experiment). First we test

our method using NavTeQ and TeleAtlas aligned maps. Subsequently we report the behaviour of our method with usual biased map data. Please note that in these tests the vehicle stops at the 4-way junction for 70 s (between the 40th and the 110th second).

Figure 3 Results of the candidate segment extraction stage

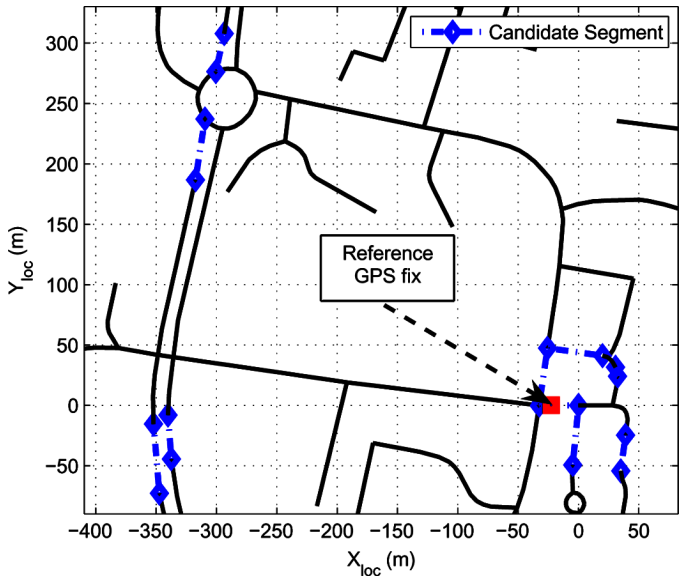

Figure 4 Results of the integrity test applied on the candidate segment of Figure 3

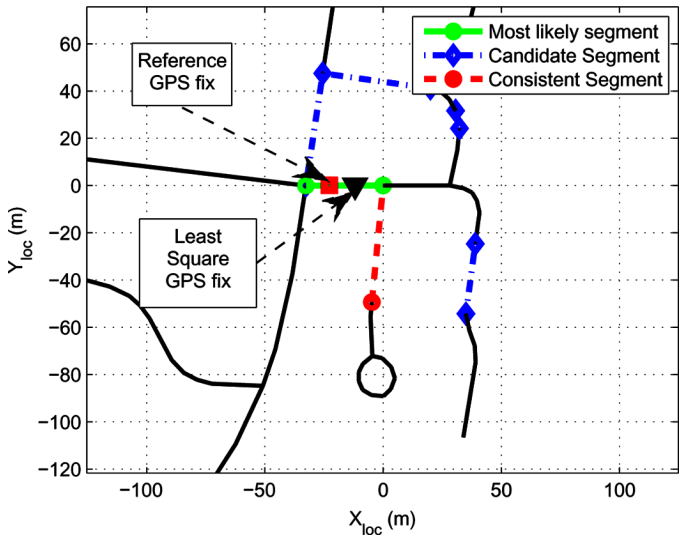

6.3.1 Tests with aligned maps

The map biases are removed in this section, with only translations given. The results of the road selection and the positioning computation are presented in Figures 5 and 6,

using aligned road caches and five visible satellites. As can be seen, in these circumstances our method yields interesting results (see Table 1).

Figure 5 Matched path, positioning residuals for the selected segment and number of candidate segments for aligned road maps. Results for map_1

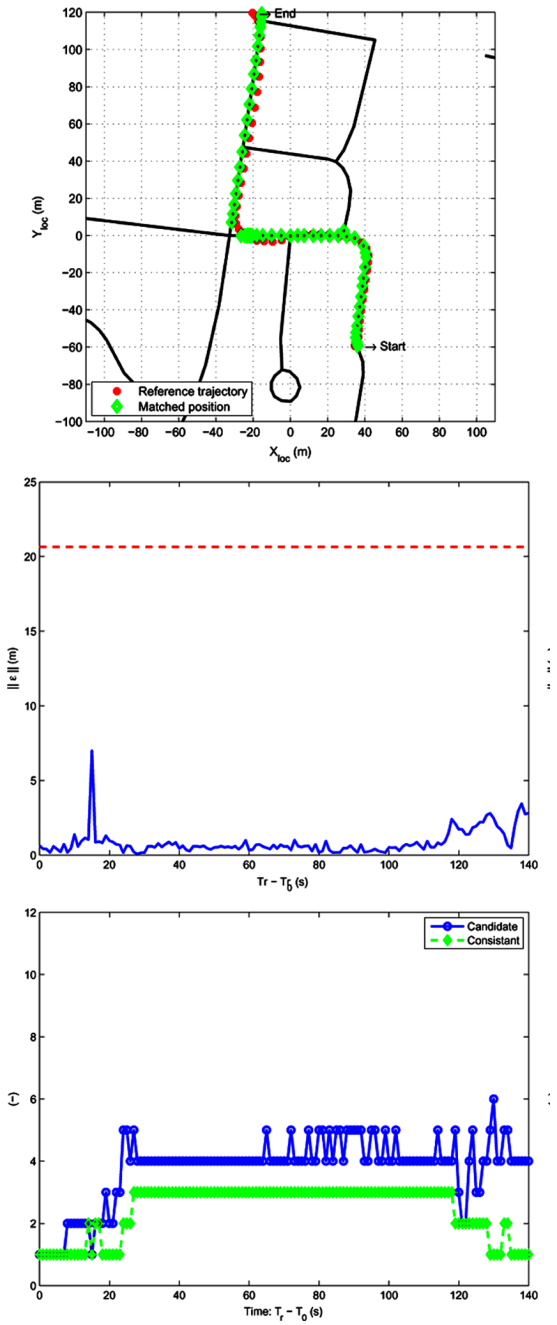

Figure 6 Matched path, positioning residuals for the selected segment and number of candidate segments for aligned road maps. Results for map_2

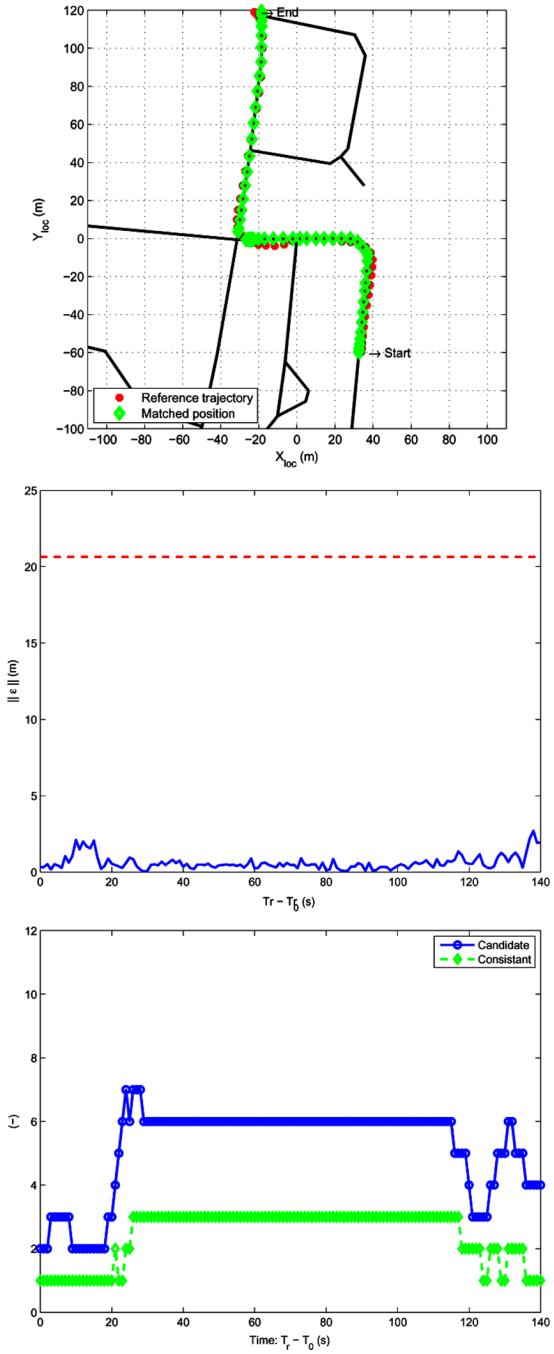

In the case of map_1, a mismatched position occurred when the first road junction was encountered, and three other mismatches appeared between the starting point and this

junction, where the road is depicted by numerous small segments. The conclusion is that in this ambiguous situation an incorrect road segment was chosen because the vehicle's true segment failed to feature among the candidates. Looking at the norm of the positioning residuals we notice a peak around second 17 after the start. This peak value corresponds effectively to the mismatch. Unfortunately, the norm of the residuals falls below the integrity threshold, and so the mismatch was not detected. Throughout the test one remarks that the value of the residuals norm remains low, that is to say around 1 meter up until the 120th second, and around 3 m afterwards, which is very good.

Table 1 Performance results using aligned maps

	No segment available (%)	*Miss-match* (%)	*True segment is consistent* (%)	*True segment is candidate* (%)
map_1	0	2.84	97.16	97.16
map_2	0	0	100	100

In the case of map_2, no mismatched position was detected. Considering the position residuals, we notice that the value of $\|\varepsilon\|$ is around 1 m, which corresponds to the pseudo-range noise. The first peak on the residuals $(10 < t < 20)$ is due to the effect of map inaccuracy, since only one segment is used to describe the curve. The second peak $(135 < t < 140)$ is due to the vehicle leaving the road and entering the parking lot.

Let us now examine the number of candidate segments extracted during these tests. Recall that the vehicle remains stationary at the 4-way junction for $40 < t < 110$. We can see that these numbers are different depending on the map used: map_1 involves on average 4 segments, where map_2 involves 6. This can be explained by the fact that the second map has smaller segments.

Regarding the selection of consistent segments, we can see that there is always at least one consistent road. On average, 2 or 3 are declared consistent, which indicates that the method hesitates often. This conclusion suggests either that the data-association strategy is over-cautious, or that the selection is difficult to assess.

6.3.2 Tests with real biased maps

In practice road maps are often biased, and usually this bias is less than 10–15 m. In this section the road selection is tested with the original NavTeQ and TeleAtlas maps in order to evaluate the effect of these offsets. Note that the two maps have different biases: map_1 is biased to the East whereas map_2 is biased to the North. Figure 7 (resp. Figure 8) depicts the results of the road selection and the matched positions using map_1 (resp. map_2).

Let us now examine the results for map_1. One can see, despite the map bias, that the map-matched locations are mainly correct. Several mismatches ($\sim$7.8% see Table 2) appear close to the different road junctions that naturally create zones of ambiguity. When looking at the positioning residuals norm one notices several interesting phenomena. The first peak value corresponds to the first one observed in Section 6.3.1: a mismatch at the first junction. The second is due to the loss of tracking

of a satellite through visibility degradation ($t \sim 125$). It should be noticed that the integrity threshold also decreases since there are only four satellites remaining at this particular instant. Another interesting point is the gap in the residuals. At time $t \sim 130$ no segment passed the integrity test and no position was computed. Finally, we can see that the average level of the positioning residuals norm is about 9 m. It corresponds effectively to the norm of the bias of the map.

Figure 7 Matched path, positioning residuals for the selected segment and number of candidate segments for original road maps. Map_1 (bias: ~ 9 m)

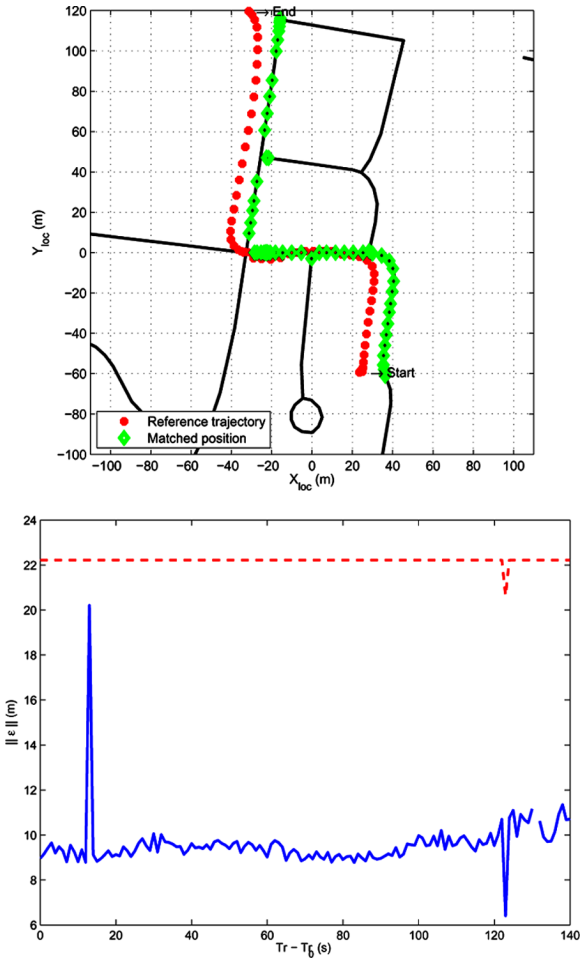

Regarding the results obtained with map_2, one remarks here that the method produces a large number of mismatches ($\sim 29\%$, as shown in Table 2). Recall that no information about previously-selected segments is used in the road selection: a new road segment selection is recomputed at each fix. Considering the positioning residuals one notices, at the beginning of the test ($t \sim 15$), that no segment is consistent for several steps. Like for the first map, we can see the loss of the tracking of an SV has an impact on the consistency. At this particular step, the loss of a satellite decreases the GPS error so that a correct road selection can be obtained. This surprising phenomenon

indicates that the satellites which disappeared was affected by a large error due to its low elevation. During the static part, close to the crossroads, we see that the average value of the positioning residual norm is 14 m, corresponding to the map bias (∼14.5 m), and the true segment is considered as the most likely segment.

Figure 8 Matched path, positioning residuals for the selected segment and number of candidate segments for original road maps. Map_2 (bias: ~ 14.5 m)

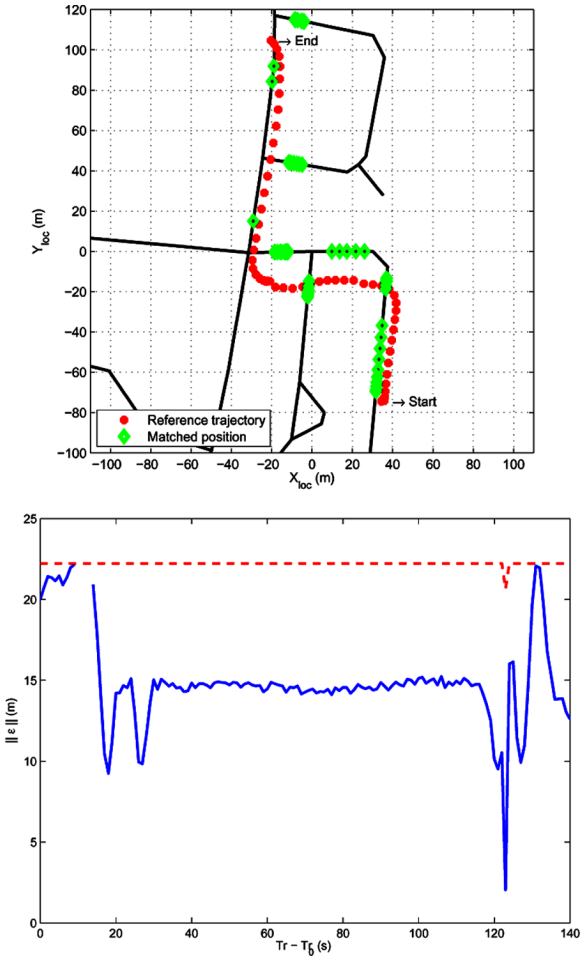

Table 2 Performance results using original maps

	No segment available (%)	*Miss-match* (%)	*True segment is consistent* (%)	*True segment is candidate* (%)
map_1	0.71	7.80	95.74	95.74
map_2	2.84	29.08	83.69	87.23

Finally, these two tests reveal (Table 2) that the true segment is considered as consistent most of time for both maps, which indicates that the integrity test is useful even if

the zero-mean noise assumption is largely violated in this experiment. Because of map bias, the true segment (i.e., the solution) is eliminated by the consistency test from the candidate segment list. This unfortunate phenomenon occurs only for map_2 'its frequency is 3.5%' as illustrated by the second line of Table 2. Therefore, we can conclude that the most likely segment selection presented in Section 5.3 is excessively discriminant when working with biased GIS data. A more efficient map-matching procedure needs to be found in this case.

7 Conclusion and future work

In this paper we have described a method to fuse road map data with GNSS rough measurements (L1 pseudo-ranges). This approach has several advantages. Since the selection of a segment is necessary, the map-matching problem can be solved using the residuals of the Newton-Raphson computation. A particular difficulty arises from the need to estimate the locations of the satellites using real-time ephemerid data in a frame attached to the map. We have proposed a method that assumes that the clock drift of the receiver is small, and consequently that the position of the satellites at their transmission times can be easily determined in a working frame attached to the map, before solving the non-linear problem. This is crucial from the practical point of view, since the satellites' locations are computed once at each stage. Therefore, the non-linear positioning problem with each segment is solved faster. In order to solve the segment selection problem, we have proposed an integrity-oriented search strategy. We have presented the computation of the consistency threshold using weighted residuals, which is essential when considering SBAS corrections. The results that we have obtained in stand-alone GPS are very encouraging, since the method is able to retrieve the correct segment if the maps are unbiased (only one incorrect match occurred using one map, and none with the other). When using real biased maps, the performance unsurprisingly decreases and the method outputs several false matches. In this case, the difficulty of the problem is observable on the residuals norm that is in the order of the map bias.

The perspectives of this research concern the use of multiple-hypothesis dynamic state observers (based on Kalman filters) to exploit the connectedness of roads, particularly when approaching junctions. Moreover, we plan also to test the use of our method with WAAS/EGNOS corrections as a means of increasing its reliability.

Acknowledgements

This research was carried out within the framework of the European FP6 Integrated Cooperative Vehicle Infrastructure Systems (CVIS) Project, launched in February 2006 for a duration of four years.

References

Belabbas, B. and Gass, F. (2005) 'RAIM algorithms analysis for a combined GPS/Galileo constellation', *ION GNSS 2005*, Los Angeles, CA, USA.

Betaille, D., Maenpa, J., Euler, H. and Cross, P. (2003) 'A new approach to GPS phase multipath mitigation', *ION National Technical Meeting – NTM2003*, Anaheim, CA, USA, pp.243–253.

Cui, Y. and Ge, S. (2003) 'Autonomous vehicle positioning with GPS in urban canyon environments', *IEEE Trans. on Rob. and Aut.*, Vol. 19, pp.15–25.

Fouque, C. and Bonnifait, P. (2007) 'Vehicle localization in urban canyons using geo-referenced data and few GNSS satellites', *IFAC Symposium on Intelligent Autonomous Vehicle – IAV2007*, Toulouse, France.

Georgiev, A. and Allen, P.K. (2004) 'Localization methods for a mobile robot in urban environments', *IEEE Trans. on Rob. and Aut.*, Vol. 20, pp.851–864.

Jabbour, M., Bonnifait, P. and Cherfaoui, V. (2006) 'Management of landmarks in a GIS for an enhanced localisation in urban areas', *IV2006 IEEE In. Veh. Symp.*, Tokyo, Japan.

Kaplan, E.D. (1996) *Understanding GPS: Principles and Applications*, Artech House, Boston.

Lahrech, A., Boucher, C. and Noyer, J-C. (2005) 'Accurate vehicle positioning in urban areas', *The 31st Annual Conference of the IEEE Industrial Electronics Society – IECON 2005*, Raleigh, NC, USA.

Laneurit, J., Chapuis, R. and Frédéric, C. (2005) 'Accurate vehicle positioning on a numerical map', *Int. J. Control, Automation and System*, Vol. 3, No. 1, pp.15–31.

Meizel, D., Renault, S. and Le Meur, A. (2005) 'GPS/GIS localization for management of vision referenced navigation in urban environments', *IEEE Conference on Intelligent Transportation Systems – ITSC2005*, Vienna, Austria.

Santa, J., Ubeda, B., Toledo, R. and Skarmeta, A. (2006) 'Monitoring the position integrity in road transport localization based services', *IEEE Vehicular Technology Conference – VTC2006*, Montreal, QC, Canada, pp.1–5.

Syed, S. and Cannon, M. (2005) 'Map-aided GPS navigation', *GPS World*, Vol. 16, No. 11, pp.39–44.

Walter, T. and Enge, P. (1995) 'Weighted RAIM for precision approach', *ION GPS*, Palm Springs, CA, USA.

Yang, M. and Chen, K-H. (2001) 'Performance assessment of a non-iterative algorithm for global positioning system (GPS) absolute positioning', *Proc. Natl. Sci. Counc. ROC(A)*, Vol. 25, pp.102–106.